Resonance effect on inverse-photoemission spectroscopy of $CeRh_3$, $CePd_3$, and $CeSn_3$

K. Kanai, Y. Tezuka, T. Terashima, Y. Muro, and M. Ishikawa
Institute for Solid State Physics, University of Tokyo, 7-22-1 Roppongi, Minatoku, Tokyo 106-8666, Japan

T. Uozumi
College of Engineering, Osaka Prefecture University, Sakai 599-8531, Japan

A. Kotani
Institute of Solid State Physics, University of Tokyo, 7-22-1 Roppongi, Minatoku, Tokyo 106-8666, Japan

G. Schmerber, J. P. Kappler, and J. C. Parlebas
IPCMS-GEMME (UMR 7504 CNRS), Université Louis Pasteur, 23, rue du Loess, 67037 Strasbourg, France

S. Shin
Institute for Solid State Physics, University of Tokyo, 7-22-1 Roppongi, Minatoku, Tokyo 106-8666, Japan
(Received 6 October 1998; revised manuscript received 23 November 1998)

The resonant inverse photoemission study (RIPES) at the Ce $4d \rightarrow 4f$ absorption edge of $CeRh_3$, $CePd_3$, and $CeSn_3$ has been carried out. The RIPES spectra show the wide variety of the $4f$ electron character in these compounds, indicating the characteristic Kondo temperature and $4f$ electron number. The excitation energy dependence of $4f$-spectral resonance, especially in $4f^2$ final-state structure, indicates a large $4d$-$4f$ multiplet splitting and strict selection rule in the final state of the RIPES process. Constant final-state spectra of the f^1 final state show the $4f$ spin-orbit splitting components. A calculation is carried out by the impurity Anderson model with full multiplet effects and explains well the excitation energy dependence of the RIPES spectra. [S0163-1829(99)04231-9]

I. INTRODUCTION

It is well known that Ce compounds show interesting electronic properties, which are mainly caused by partially localized character of $4f$ electrons. Some Ce compounds form so-called valence fluctuation (VF) systems, where $4f$ electrons have itinerant character because of strong hybridization with the band electrons. In VF systems, the ''Kondo resonance'' is known to be observed just above the Fermi level through inverse photoemission spectroscopy (IPES). Therefore, IPES is a very suitable method to investigate the electronic structure of such Ce compounds.

Resonant inverse photoemission spectroscopy (RIPES) is a new technique to investigate the unoccupied electronic states of solids. Recently, Weibel *et al.*[1] have performed RIPES measurements of several Ce compounds near the Ce-M_5 edge. Kanai *et al.*[2] have also measured the RIPES of $CePd_7$ near the Ce-$N_{4,5}$ edges. The great ability to study the $4f$ electronic structure by resonant enhancement of the $4f$ signal was testified. In these studies, the measurements have been performed on Ce $3d \rightarrow 4f$ and $4d \rightarrow 4f$ absorption edges. The $4f$ cross section increases when the excitation energy is tuned to the Ce-M_5 and -$N_{4,5}$ absorption edges, so that the Ce-$4f$ contribution can be extracted. In the $N_{4,5}$ case, the normal IPES process for the transition to Ce $4f$ states is represented as follows:

$$|4d^{10}4f^n\rangle + e^- \rightarrow |4d^{10}4f^{n+1}\rangle + h\nu. \quad (1)$$

Here, n is the configuration number of the $4f$ electrons in the initial state. For the incident-energy range of the present experiment, a large contribution from non-f conduction bands (Ce-$5d$ band) also coexists with the f contribution in the normal IPES. In the RIPES experiment, on the other hand, resonant processes are expressed by the following super Coster-Kronig processes:

$$|4d^{10}4f^n\rangle + e^- \rightarrow |4d^{9}4f^{n+2}\rangle \rightarrow |4d^{10}4f^{n+1}\rangle + h\nu. \quad (2)$$

Since the initial and final states are the same in these two processes (1) and (2), they interfere with each other. Therefore, the $4f$ cross section increases when the excitation energy (E_{ex}) is tuned to Ce $4d \rightarrow 4f$ absorption edge. We can extract the Ce $4f$ contribution by using RIPES process.

There are two types of resonance in Ce compounds according to the $3d$ or $4d$ absorption edges. The process of Eq. (2) is the super Coster-Kronig transition at the $4d$ absorption edge, and the corresponding process at $3d$ absorption edge is the normal Coster-Kronig transition. Thus, the resonance effect by super Coster-Kronig transitions is strong at $4d$ absorption edge, while the incoherent process such as the normal fluorescence is strong at $3d \rightarrow 4f$ threshold. In fact, a clear resonant effect was observed at Ce-$N_{4,5}$ absorption edge and several different features from that of M_5 edge were pointed out.[2]

In this paper, the RIPES near the Ce-$N_{4,5}$ absorption edge of cubic crystal structure of $AuCu_3$-type compounds, $CeRh_3$, $CePd_3$, and $CeSn_3$, are reported. These compounds are known as typical VF systems and have different $4f$ hybridization strengths.[3] The RIPES near Ce-M_5 absorption edge of $CeRh_3$ and $CePd_3$ were performed in Ref. 1. The purpose

of this paper is to investigate the resonance effect by analyzing the RIPES spectrum near $N_{4,5}$ edge. A calculation is performed in the framework of the impurity Anderson model with full multiplet coupling effects.

II. EXPERIMENT

The polycristalline samples were synthesized by arc melting the stoichiometric amounts of the constituents on a water-cooled copper hearth under a flowing purified argon atmosphere. To improve the homogeneity, for $CePd_3$ and $CeRh_3$ the buttons were turned over and remelted six times, then splat cooled to large surface and $CeSn_3$ ingot was annealed in an evacuated quartz tube at 950 °C for 4 days followed by an additional annealing at 900 °C for 10 days. Conventional x-ray examination was carried out on these samples with Cu $K\alpha$ radiation. The crystal structure has been confirmed to be of $AuCu_3$ type.

Measurements were performed in an ultrahigh vacuum chamber where the base pressure was about 5×10^{-11} Torr. Samples were kept around 25 K by closed cycle ^{4}He refrigerator. Clean sample surfaces were obtained by scraping the surface with a diamond file in a high vacuum every 10 $\sim$40 min at 25 K. A thermal cathodetype electron gun (employing BaO for cathode) was used for the excitation source. The kinetic energy $E_{\rm ex}$ of the electron was calibrated by the electron energy analyzer. The IPES was measured by the soft x-ray emission system, which has a Rowland mountedtype spectrometer.[4] The Fermi-level position and an energy resolution of the system were determined by referring to the Fermi edge in the IPES spectra of Au, which was evaporated on the sample holder. Energy resolution of this system is 0.44 eV at $E_{\rm ex}=90$ eV and it was found that $E/\Delta E\sim200$ in the wide energy range in this system.

III. THEORETICAL MODEL

The RIPES is analyzed by means of an impurity Anderson model with full multiplet coupling effects in a Ce ion. Our system is composed of Ce $4f$, $4d$ core and conduction-band states (only states below the Fermi level E_F are taken into account in the present analysis), and is described by the Hamiltonian,

$$H=\varepsilon_f\sum_\gamma f_\gamma^+ f_\gamma+\sum_{k,\gamma}\varepsilon_v(k)a_{k\gamma}^+a_{k\gamma}+\frac{V}{\sqrt{N}}\sum_{k,\gamma}(f_\gamma^+a_{k\gamma}+a_{k\gamma}^+f_\gamma)+U_{ff}\sum_{\gamma>\gamma'}n_{f_\gamma}n_{f_{\gamma'}}-U_{fc}\sum_{\gamma,\xi}n_{f_\gamma}c_\xi c_\xi^+ +H_{\rm mult}, \tag{3}$$

where $f_\gamma^\dagger$, $c_\xi^\dagger$, and $a_{k\gamma}^\dagger$ are the electron creation operators for $4f$, $4d$ core, and conduction states, respectively, the indices γ and ξ represent both orbital and spin states and k denotes the discrete energy levels of conduction band below E_F ($k=1,\ldots,N$). The first and second terms describe the one-particle energy of $4f$ and conduction electrons, where the latter is expressed, with the energy width W from the bottom of conduction band to the Fermi level E_F and with a rectangular density of states, as

$$\varepsilon_v(k)=\varepsilon_v+\frac{W}{N}\left(k-\frac{N+1}{2}\right). \tag{4}$$

The third term describes the hybridization effect between $4f$ and conduction states. It should be mentioned that the configuration-dependent hybridization strength with $(R_c,R_v)=(0.7,0.8)$, following Ref. 5, is used in the present analysis, although that is not explicitly taken into account in Eq. (3). The fourth and fifth terms describe the $4f$-$4f$ interaction and $4f$-core attractive potential, respectively. The last term $H_{\rm mult}$ contains multipole parts of the Coulomb interaction, described in terms of Slater integrals, and the spin-orbit coupling effect. The Slater integrals F^k and G^k and the spin-orbit coupling constants $\zeta(4f)$ and $\zeta(4d)$ are estimated through the Hartree-Fock-Slater calculation for Ce ion.

The present RIPES analysis is made only for $CeRh_3$. The parameters of ε_f, V, U_{ff}, $U_{fc}(4d)$, and W are taken as -1.8, 0.56, 6.8, 8.4, and 4.0 eV, respectively, so as to reproduce the $3d$ core x-ray photoemission of $CeRh_3$, where the $U_{fc}(4d)$ is assumed to be 80% of the value of $U_{fc}(3d)$.

As the basis sets to describe the wave function, f^0, f^1L, and f^2L^2 electron configurations are taken into account for initial state, cf^2 and cf^3L for intermediate states and f^1, f^2L and f^3L^2 for RIPES final states, where c and L mean a $4d$ core hole and a hole in the conduction band below E_F, respectively.

Using the ground state $|g\rangle$ and the final states $|f\rangle$ obtained within the above framework, the RIPES is calculated as a function of the incident electron energy $E_{\rm ex}$ and emitted photon energy ω by

$$F(\omega,E_{\rm ex})=\sum_f\left|\left\langle f\left|T_R+T_R\frac{1}{E_{\rm ex}+E_g-H+i\Gamma}V_A^+\right|g\right\rangle\right|^2\times\delta(E_{\rm ex}+E_g-\omega-E_f), \tag{5}$$

where T_R represents the electric dipole transition and V_A^+ represents the $4d\varepsilon g$-$4f4f$ Coulomb scattering, so that the first term describes the direct IPES process $|g\rangle\rightarrow|f\rangle$, while the second term describes the resonant process through the $4d\rightarrow4f$ resonant excitation by an incident electron εg in the intermediate state. Γ is the lifetime in the intermediate state and is taken to be 2.0 eV in the present analysis.

IV. RESULTS AND DISCUSSION

The off resonant-RIPES spectra of $CeRh_3$, $CePd_3$, and $CeSn_3$ are shown in Fig. 1(a). The cross section of $4f$ level for inverse photoemission reaches its maximum around 80 $\sim$90 eV. Therefore, the spectra in Fig. 1(a) are measured around $E_{\rm ex}=80$ eV to obtain larger $4f$ contribution. Obviously, the considerable variations of the off-resonant spectra indicate the difference of their unoccupied states. The strong peak at 1.1 eV above Fermi level in the spectrum of $CeRh_3$ is ''f^1 peak,'' which corresponds to the $4f^1$ final state. It is known that the f^1-peak structure contains the Kondo resonance. However, the spin-orbit and crystal field splitting of $4f^1$ final state are convoluted with the experimental energy

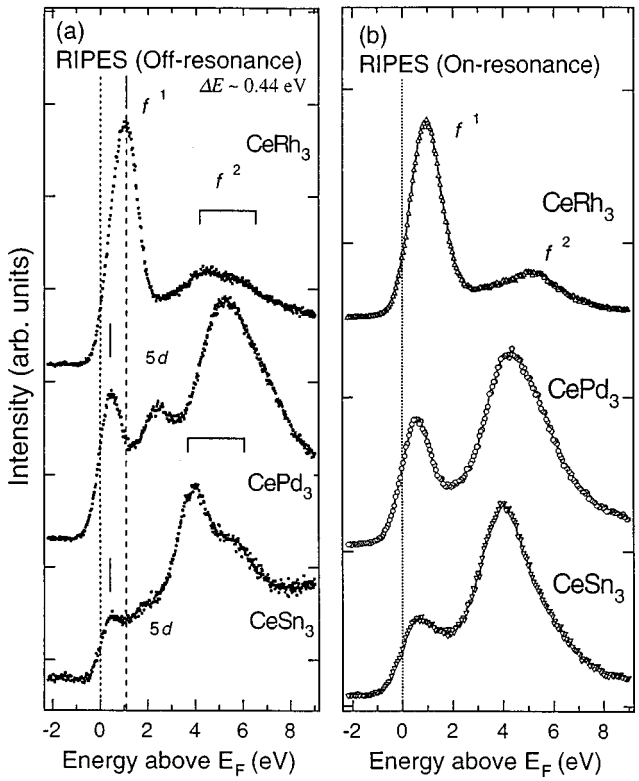

FIG. 1. (a) The off resonant RIPES spectra of $CeRh_3$, $CePd_3$, and $CeSn_3$. The abscissa is the energy above Fermi level (E_F). The measurements were performed at 25 K and about 80 eV of E_{ex}. (b) The on-resonant RIPES spectra of $CeRh_3$, $CePd_3$, and $CeSn_3$.

resolution in the f^1 peak. Thus, the present f^1-peak position in the experiment does not exactly show Kondo temperature, T_K, though the peak energy of 1.1 eV is much larger than the experimental resolution in $CeRh_3$. It is thought that Kondo resonance is situated at the lower-energy side of the f^1 peak; as discussed later, the low-energy side component in f^1 peak of $CeRh_3$ is situated at 0.78 eV above E_F.

The f^1 peaks of $CePd_3$ and $CeSn_3$ in Fig. 1(a) are located at 0.5 eV. However, the f^1 peaks of $CePd_3$ below the $4d$ threshold split into two states, as shown in Fig. 2. This splitting is thought to be due to the spin-orbit splitting of $4f$ level. The splitting energy is about 0.3 eV. The energy position of lowest f^1 state is around 0.45 eV. The T_K's of $CePd_3$ and $CeSn_3$ are around 200 K so that the energy position of f^1 states are mainly determined by the energy resolution for those materials.

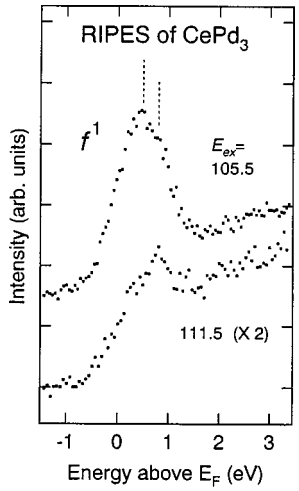

FIG. 2. The RIPES spectra of $CePd_3$ at prethreshold region. The dotted lines indicates the spin-orbit component in the f^1 peaks.

It is obvious that the f^1 peak of $CeRh_3$ has much stronger intensity and which is located in higher energy than those of $CePd_3$ and $CeSn_3$. This indicates the extremely high T_K and strong itinerant character of $4f$ electron of $CeRh_3$. This result is consistent with the extremely low values of Pauli-like magnetic susceptibility $\chi_0 = 0.31(10^{-3}$ emu/mol) at 0 K, and the ratio χ_0/γ of 0.022 (emu K^2/J), though typical Ce compounds in its VF state have an enhanced χ_0 in the range of $0.5 \sim 1$ (10^{-3} emu/Ce atom) (Ref. 6) and a ratio χ_0/γ of 0.035 (emu K^2/J).[7] The $CePd_3$ and $CeSn_3$ have nearly the same T_K, which may explain the similar physical properties of $CePd_3$ and $CeSn_3$.[8]

The structures corresponding to the final state with $4f^2$ configuration are observed around 5 eV in the spectra of $CeRh_3$ and $CePd_3$ and 4 eV in $CeSn_3$. These broad peaks are called ''f^2 peak.'' The intensity ratio of the f^1 peak to the total $4f$ intensity is denoted by r_f

$$r_f \equiv \frac{I(f^1)}{I(f^1)+I(f^2)}. \tag{6}$$

Here, $I(f^n)$, $(n=1,2)$ represents the integrated intensity of f^n peak. The r_f strongly reflects an average number of $4f$ hole, $1-n_f$, where n_f is an average number of $4f$ electron, and can be regarded as a good index for the itinerant character of these systems. The f^2 peaks are found to have several multiplet components in the spectra of $CeRh_3$ and $CeSn_3$. For $CeRh_3$, the peak at 4 eV and the shoulder at 5 eV corresponds to the multiplet structures with f^2 configuration. The same structures for $CeSn_3$ are found at 4 and 5.5 eV, respectively. The peak at the lower-energy side (at 4 eV for both) can be thought to be made up by the triplet final state.[10] In fact, the lowest energy multiplet of $^3H_4$ has large spectral weight. Because of the exchange interaction, the parallel coupling between $4f$ spins lowers the final-state energy under the Hund's rule. The structures at 2 eV in the spectra of $CePd_3$ and $CeSn_3$ are assigned to be the Ce-$5d$ band by comparison with the band calculation.[11] It seemed to be cumbersome to estimate the positions and integrated intensities of the f^1 and f^2 peaks without ambiguity by subtracting the non-f background (mainly, Ce-$5d$ band and ligand $4d$ band). This problem can be solved by using the following resonant effect.

Figure 1(b) shows the on-resonant RIPES spectra of $CeRh_3$, $CePd_3$, and $CeSn_3$. The excitation energies E_{ex} are chosen in order to drastically enhance the f^1 peak for each system. The Ce-$5d$ band is not found in the spectra of $CePd_3$ and $CeSn_3$ due to the dramatic enhancement of $4f$ components. Reduction of spectral intensity at Fermi level in the on-resonant spectrum of $CeRh_3$ is caused by the reduced $5d$-band contribution just above Fermi level by the resonance effect. Thus, the on-resonance spectra in Fig. 1(b) can be regarded as the $4f$ contribution itself.

It is found that f^1 peak intensity of $CeRh_3$ is extremely large in comparison with the corresponding intensity of

TABLE I. The RIPES peak intensities ratio, r_f and $c(f^0)$ derived from analyses of $3d$-XPS data for $CeRh_3$, $CePd_3$, and $CeSn_3$. The number in the parenthesis for $CeRh_3$ is $c(f^0)$ derived from the theoretical analysis in this paper.

	r_f	$c(f^0)(3d\text{XPS})$
$CeRh_3$	0.60	0.26 (0.20)
$CePd_3$	0.22	0.08
$CeSn_3$	0.18	<0.05

$CePd_3$ and $CeSn_3$. Furthermore, the intensity at Fermi level is small. This is consistent with the extremely low value of χ_0 of $CeRh_3$ obtained by other experiments. The remarkable itinerant character of $4f$ electron of $CeRh_3$ is supplemented with the strongly depressed f^2 peak. The $CeRh_3$ can be regarded as the most α-like metallic Ce compound. Similar remarkable properties are reported for $CePd_7$.[12]

The f^1 peak of $CeSn_3$, which is not seen clearly in off-resonant spectrum in Fig. 1(a) appears distinctly in on-resonance one in Fig. 1(b). The peak intensity ratio r_f that are represented in Eq. (6), is estimated in Table I. The T_K of $CePd_3$ has been reported to be about 240 K (Ref. 9) and that of $CeSn_3$ to be about 200 K. They have very similar Kondo temperatures. It is interesting that r_f of $CeSn_3$ is smaller than that of $CePd_3$ irrespective of similar T_K. This fact mainly indicates the reduction of the strength of $4f$ hybridization in $CeSn_3$. This difference of hybridization strength between $CePd_3$ and $CeSn_3$ is caused by much larger nearest-neighbor Ce-Ce distance in $CeSn_3$ (4.72 Å) than in $CePd_3$ (4.13 Å) in the same $AuCu_3$-type crystal structure.[8] The Kondo temperature T_K that rules the low-energy properties, depends on these parameters, ε_f, U_{ff}, hybridization strength V, and the degeneracy of the $4f$ level. As a result of the balance of these parameters, similar physical properties of $CePd_3$ and $CeSn_3$ originate from similar T_K's which are roughly estimated from the energy positions of the f^1 peaks in Fig. 1(b). They have very similar Kondo temperatures T_K. However, it should be pointed out that the f-peak intensity ratio r_f in Table I is quite different for $CePd_3$ and $CeSn_3$. Let us discuss why the RIPES spectra of $CePd_3$ and $CeSn_3$ are so different, though they have a similar value of T_K. As shown by Bickers, Cox, and Wilkins,[13] the transport and thermodynamic properties of mixed valence Ce systems are represented by universal functions scaled by T_K, but it should be noted that the high-energy properties such as the ratio r_f are not scaled only by T_K. According to our preliminary calculation, if we change ε_f and V simultaneously so as to keep T_K (f^1-peak position) unchanged, the value of r_f can be changed. We can say that T_K depends on ε_f, U_{ff}, and V, but different combinations of these quantities can change r_f with T_K kept constant.

It is also to be noted that there is another possibility to explain almost the same T_K and the different r_f for $CePd_3$ and $CeSn_3$. In our discussion, we have tentatively disregarded the surface contribution to RIPES, but actually the RIPES at the $4d$ threshold should have a considerable surface sensitivity. It is known that the valence number of a Ce ion in surface layers can be different from that in the bulk system because of the reduction of the coordination number.

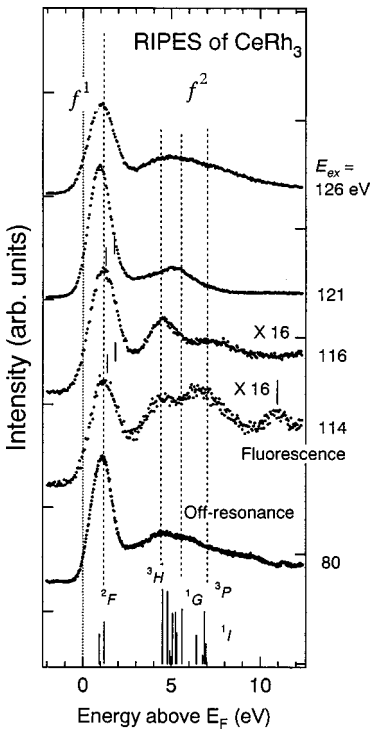

FIG. 3. The RIPES spectra of $CeRh_3$ at several excitation energies. The numbers written on the side of the right axis represent E_{ex}. The calculated multiplets in $4f^1$ and $4f^2$ final-state configurations are added at the bottom axis. The structure indicated by vertical bar in the spectrum at $E_{ex}=114$ eV is the normal fluorescence.

Therefore, if we assume that the surface contribution to RIPES is different for $CePd_3$ and $CeSn_3$, then the different r_f value can be explained even with the same T_K value in the bulk system.

The r_f of $CeRh_3$ is much larger than those of $CePd_3$ and $CeSn_3$. The $c(f^0)$ which is the f^0 weight in the ground state is derived from analyses of $3d$-x-ray photoemission spectroscopy (XPS) data[14] for $CeRh_3$, $CePd_3$, and $CeSn_3$ and listed in Table I. The $c(f^0)$ is not $1-n_f$ itself because of a small f^2 contribution in the ground state. It may introduce a small error to regard $c(f^0)$ as $1-n_f$. r_f is larger than $c(f^0)$. This is caused by the following two reasons: one is that r_f was estimated in the spectrum measured at the energy where the f^1 peak is most enhanced and then the intensity of the f^1 peak was overestimated; the other is that the stronger hybridization strength of f^1 and f^2 configurations in the final state transfers the spectral weight from the f^2 to f^1 final state. It is emphasized that the ratio of the three r_f's 0.60:0.22:0.18 is similar to that of $c(f^0)$ 0.26:0.08:0.05, respectively for $CeRh_3$, $CePd_3$, and $CeSn_3$. Therefore, the r_f can provide good information about the itinerant character of $4f$ electron in the initial state.

The f^2 spectrum in Fig. 1(b) exhibits a single peak without the shoulders observed in off-resonant spectra in Fig. 1(a). For $CeRh_3$ and $CeSn_3$, the f^2 peaks are located at about 4.8 and 4.0 eV, respectively. The reason for the lack of the other f^2 components is explained by considering the selection rule in the final state of RIPES process.[10] Figure 3 shows the excitation energy dependence of RIPES spectra of $CeRh_3$. The multiplet structures are indicated by the vertical bars and dashed lines in Fig. 3. A dramatic change in spectral

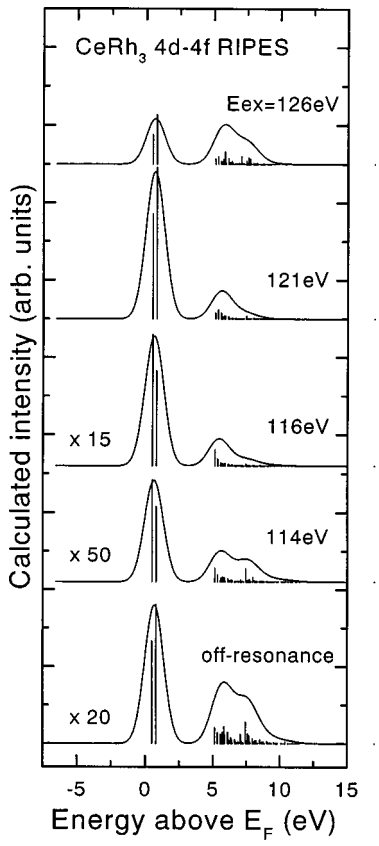

FIG. 4. Calculated $4d$-$4f$ RIPES with various excitation energy E_{ex} and off-resonant IPES spectra (bottom). The multiplet structures are also shown by thin lines.

line shape of f^2 peak is observed as the excitation energy changes. This is caused by the transfer of spectral weight among the multiplet structures at the f^2 final states. In order to interpret this excitation energy dependence of f^2 peak, we have to take the selection rule in the final state on resonance into account. The f^1 peak consists of spin-orbit components in the $4f^1$ final state, which are separated by about 0.3 eV. It is found that the two components of f^1 peak are clearly observed in the spectra of $CePd_3$ at prethreshold region, $E_{ex}=105.5$ and 111.5 eV, as shown in the Fig. 2. The $^2F_{5/2}$ and $^2F_{7/2}$ multiplet structures in the f^1 peak are indicated by dotted lines. The spectral intensity of the $^2F_{5/2}$ structure transfers to $^2F_{7/2}$ structure as E_{ex} increases. This suggests a strong excitation energy dependence of the $^2F_{5/2}$ and $^2F_{7/2}$ multiplet structures. This splitting is also found in $CeRh_3$, as shown in Fig. 3, though they are broad. The excitation energy dependence of the f^1 peak of $CeRh_3$ is discussed later.

Figure 4 shows the calculated RIPES with the excitation energies corresponding to those in Fig. 3 and the off-resonant IPES in the bottom of the figure. In this figure, the vertical lines are calculated by Eq. (5) and show clear multiplet structures, while the continuous spectra are obtained by convoluting them with a Gaussian function of width $\Gamma_G=0.8$ eV [half width at half maximum (HWHM)] in order to include the overall resolution. It is shown that the experimental RIPES in Fig. 3 are fairly well reproduced by the calculation at various excitation energies. Especially the dramatic transfer of spectral weight on the resonantly enhanced multiplet structures at the f^2 final states is explained well. In

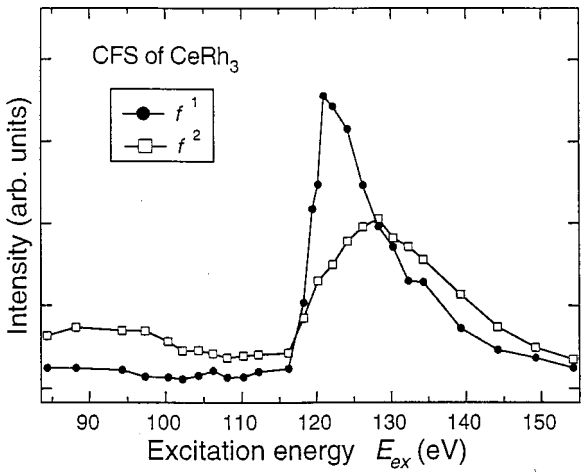

FIG. 5. The CFS spectra for the $4f^1$ and $4f^2$ final states. The spectrum was obtained by plotting the integrated intensities of f^1 and f^2 peaks against the excitation energy E_{ex}.

Fig. 3, in the off-resonant spectra at $E_{ex}=80$ eV all $4f^2$-multiplet components are blurred with the experimental resolution and not obviously distinguished. The broad band of multiplet structures at the f^2 final states in calculated off-resonant spectrum (Fig. 4) corresponds to this. In the spectrum at $E_{ex}=114$ eV, which is in the region of the prethreshold of the Ce $4d\rightarrow 4f$ absorption, f^2 peak is clearly split into two peaks. These two peaks are also reproduced in the calculation and are roughly assigned to ^3H and ^3P components. Discrepancy of the f^2 peak intensities of ^3H and ^3P components between experimental and calculated result may be accounted for by taking the background and surface contribution into account. The spectral weight of ^3P component is weakened as the excitation energy increases from 116 to 126 eV in Fig. 3. The multiplets around 5 eV ($^3H\sim{}^1G$) are resonantly enhanced though the multiplets at higher-energy side ($^1D\sim{}^1I$) are not found at $E_{ex}=126$ eV, where the f^1 peak is the most enhanced. On the other hand, the ^1G component seemed to be enhanced in the spectrum at 121 eV. Finally, the spectral line shape at $E_{ex}=126$ eV resembles that at 80 eV. This excitation energy dependence of RIPES spectrum is well explained by the calculated results in Fig. 4. At $E_{ex}=121$ eV, the resonance spectrum has a clear resonance peak at 5.5 eV above E_F between ^3H and ^3P structures. That is, there are three enhanced multiplet structures in the f^2 state. To understand the excitation energy dependence of the resonance effects on the multiplet components, the following intuitive discussion is presented.[10] In the off-resonant region the selection rule of the $4f^1\rightarrow 4f^2$ IPES transition process is not strict, i.e., the electrons added to the $4f$ level can have either up- or down-spin configurations. Therefore, all multiplet components corresponding to a possible final state can be observed. However, on the resonance, the intermediate state with the $4d$-hole spin occurs in RIPES process and the large multiplet splitting of ($4d^94f^3$) state concerning the arrangement of two $4f$ electrons and $4d$-hole spin springs up. The intermediate state with three up-spin $4f$ electrons and a down-spin $4d$ hole gives the lowest energy under the restriction of the selection rule for dipole transition. This intermediate state transits into the triplet final state at the resonance. The spectral intensity of f^2 peak shifts from lower

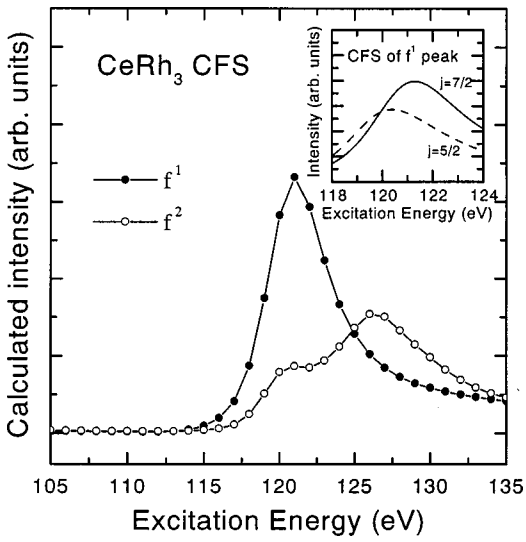

FIG. 6. Calculated CFS for f^1 (closed circle) and f^2 (open circle) final states. The inset shows the CFS for $F_{5/2}$ and $F_{7/2}$ multiplets in the f^1 final state.

energy side to higher-energy side as the excitation energy increases after the giant resonance in Fig. 3. This fact reflects the energy dependence of possible intermediate state of RIPES process. The two-peak structure of f^2 peak at prethreshold region (114 eV in Fig. 3) where the excitation energy is lower than that of giant resonance, can be interpreted by the following reason. In this energy region, there are weak intermediate states, which correspond to dipole-forbidden states. That is, the absorption, $4d^{10}4f^1+e^- \rightarrow 4d^9 4f^3$, takes place by the spin-orbit interaction through the mixing with the dipole-allowed state. Therefore, the intermediate states, which make transition to the singlet or higher triplet final state can take place.

The constant final state (CFS) spectra of RIPES in $CeRh_3$ are shown in Fig. 5. The spectra are obtained by plotting the integrated intensities of f^1 and f^2 peaks versus the kinetic energy of the electron, E_{ex}. Around 120 eV of E_{ex}, the giant resonance takes place as E_{ex} strides over the Ce $4d \rightarrow 4f$ threshold. This strong-resonance enhancements of f^1 and f^2 intensities at the $4d \rightarrow 4f$ threshold clearly show that these structures come from the localized $4f$ component. The f^1 and f^2 curves reach a maximum at about 121 and 127 eV, respectively, and slowly decrease as the excitation energy increases. The asymmetric line shapes of both curves with the dip just before the giant resonance around 100–115 eV of E_{ex} represents a very large multiplet splitting of the intermediate state and the existence of Fano-type interference. This Fano line shape has not been clearly observed in the RIPES of Ce compounds at the M_5 absorption edge.[1] This difference represents the strong-Coulomb interaction between $4d$ and $4f$ state due to a larger overlap of wave functions of both states with same principal quantum number. The calculated CFS that are integrated intensities of whole f^1 and f^2 multiplets corresponding to f^1 and f^2 final states in RIPES are shown in Fig. 6. Asymmetric line shapes, which are characteristic of the $4d$-$4f$ case of experimental CFS in Fig. 5 are well reproduced by the calculation. The broader feature of f^2 curve in the experimental result as compared to the calculated one is due to the incoherent components at the higher-energy side of E_{ex}.

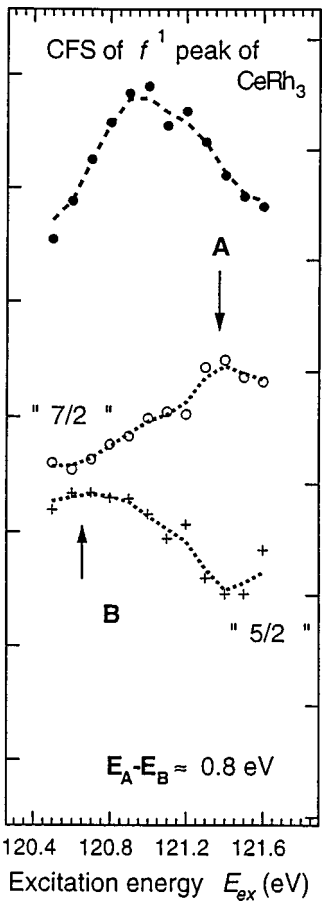

FIG. 7. The CFS spectra for the f^1 peak of $CeRh_3$, which were measured in the narrow energy range. The dotted lines are guides for the eyes. Top spectrum is the f^1 curve and middle and bottom spectra that are labeled $\frac{7}{2}$ and $\frac{5}{2}$ are the one for $^2F_{5/2}$ and $^2F_{7/2}$ final states, respectively. A and B are the maxima of $\frac{7}{2}$ and $\frac{5}{2}$ curves and E_A and E_B are the energy of A and B.

In order to derive more information from CFS spectra, the f^1 curve was measured in a narrow energy range shown in Fig. 7. It should be emphasized that the CFS spectra contain the information about the intermediate state in RIPES process. The top spectrum that indicates the total f^1 intensity has the maximum at 121.0 eV. The middle and bottom ones that are labeled $\frac{7}{2}$ and $\frac{5}{2}$ are the CFS spectra for $^2F_{5/2}$ and $^2F_{7/2}$ final states, respectively. And so, the sum of the middle and bottom spectrum intensities reproduces the top one. The maximum points of $\frac{7}{2}$ and $\frac{5}{2}$ curves are split by about 0.8 eV. The inset in Fig. 6 shows the calculated CFS for $F_{5/2}$,$F_{7/2}$ multiplets in the f^1 final state. The peak-energy separation between $F_{5/2}$ and $F_{7/2}$ spectra is shown to be about 0.9 eV and it corresponds to that of 0.8 eV in experiment of Fig. 7. This energy split can be interpreted as the difference of the intermediate state energies. In the RIPES process, the initial state $^1S_0$ transits to some intermediate states with allowed symmetry through the selection rules for Coulomb scattering. It is known that the $^2G_{9/2}$ and $^2G_{7/2}$ intermediate states make transition to the $^2F_{7/2}$ and $^2F_{5/2}$ final states, respectively. And these transitions make much contribution to $^2F_{7/2}$ and $^2F_{5/2}$ spectral intensities. Therefore, the difference of 0.8 eV between the maximum points of $\frac{7}{2}$ and $\frac{5}{2}$ curves reflects the energy separation between the $^2G_{9/2}$ and $^2G_{7/2}$

intermediate states. In practice, the $\frac{7}{2}$ and $\frac{5}{2}$ curves are thought to be broadened by the lifetime effect of the intermediate state.

It is needed to keep the surface effect in mind, because it is known that there is large surface effect in Ce compounds and the electron energy around 120 eV has a very short mean-free path. In terms of surface effect, the change of Ce-$4f$ level and the reduction of hybridization between the $4f$ and ligand extended states lead to the localization of $4f$ electron in surface region. The RIPES is a powerful method to study the surface effect, because the E_{ex}'s select the surface or bulk state and the energy dependence of E_{ex} enables to study the change of the electron mean-free path. These surface effects on RIPES will be discussed elsewhere in the near future.

V. CONCLUSION

RIPES measurements near the Ce-$N_{4,5}$ absorption edge are able to provide information about various of $4f$ states in cubic crystal structure ($AuCu_3$-type) compounds such as $CeRh_3$, $CePd_3$, and $CeSn_3$. The RIPES at the Ce $4d \rightarrow 4f$ edge was found to be a powerful method to investigate $4f$ electronic structures. The r_f estimated from RIPES spectra gave important information about the $4f$ electronic structures.

A calculation for $CeRh_3$ in the framework of the impurity Anderson model with full multiplet effects reproduced RIPES spectra and well explained the excitation energy dependence of f^1 and f^2 peak in the RIPES spectra.

[1] P. Weibel, M. Grioni, D. Malterre, B. Dardel, and Y. Baer, Phys. Rev. Lett. **72**, 1252 (1994); M. Grioni, P. Weibel, D. Malterre, F. Jeanneret, Y. Baer, and G. Olcese, Physica B **206&207**, 71 (1995); M. Grioni, P. Weibel, D. Malterre, Y. Baer, and D. Duo, Phys. Rev. B **55**, 2056 (1997); P. Weibel, M. Grioni, C. Heche, and Y. Baer, Rev. Sci. Instrum. **66**, 3755 (1995); P. Weibel, M. Grioni, D. Malterre, O. Manzardo, Y. Baer, and G. L. Olcese, Europhys. Lett. **29**, 629 (1995).

[2] K. Kanai, Y. Tezuka, M. Fujisawa, Y. Harada, S. Shin, G. Schmerber, J. P. Kappler, J. P. Parlebas, and A. Kotani, Phys. Rev. B **55**, 2623 (1997).

[3] T. Kasuya, Prog. Theor. Phys. Suppl. **108**, 1 (1992); I. Umehara, Y. Kurosawa, N. Nagai, M. Kikuchi, K. Sato, and Y. Onuki, J. Phys. Soc. Jpn. **59**, 2848 (1990).

[4] S. Shin, A. Agui, M. Fujisawa, Y. Tezuka, T. Ishii, and N. Hirai, Rev. Sci. Instrum. **66**, 1584 (1995).

[5] K. Okada and A. Kotani, J. Electron Spectrosc. Relat. Phenom. **71**, R1 (1995).

[6] A. Iandelli and A. Palenzona, in *Handbook on the Physics and Chemistry of Rare Earths*, edited by K. A. Gschneider, Jr. and L. Eyring (North-Holland, Amsterdam, 1987), Vol. X, Chap. 71.

[7] M. J. Besnus, J. P. Kappler, and A. Meyer, Physica B **130**, 127 (1985).

[8] J. G. Sereni, in *Handbook on the Physics and Chemistry of Rare Earths*, edited by K. A. Gschneider, Jr. and L. Eyring (North-Holland, Amsterdam, 1991), Vol. 15, Chap. 98.

[9] J. M. Lawrence, J. D. Thompson, and Y. Y. Chen, Phys. Rev. Lett. **54**, 2537 (1985).

[10] A. Tanaka and T. Jo, Physica B **206&207**, 74 (1995); J. Phys. Soc. Jpn. **65**, 615 (1996).

[11] S. Lukas and J. Börje, Phys. Rev. B **50**, 17 886 (1994).

[12] H. Takeya, K. A. Geshneider, B. J. Beaudry, T. Ellis, and V. K. Pecharsky, J. Alloys Compd. **209**, 35 (1994); J. G. Sereni, O. Trovarelli, A. Herr, J. Ph. Schillé, E. Beaurepaire, and J. P. Kappler, J. Phys.: Condens. Matter **5**, 2927 (1993).

[13] N. E. Bickers, D. L. Cox, and J. W. Wilkins, Phys. Rev. B **36**, 2036 (1987).

[14] J. C. Fuggle, F. U. Hilebrecht, Z. Zolnierek, R. Lässer, Ch. Feiburg, O. Gunnarsson, and K. Schönhammer, Phys. Rev. B **27**, 7330 (1983); G. Krill, J. P. Kappler, A. Meyer, L. Abadli, and M. F. Ravet, J. Phys. F **11**, 1713 (1981); E. Wuilloud, W.-D. Schneider, Y. Baer, and F. Hulliger, J. Phys. C **17**, 4799 (1984).